IOP PUBLISHING PHYSICS IN MEDICINE AND BIOLOGY

Phys. Med. Biol. **54** (2009) 1723–1742 doi:10.1088/0031-9155/54/6/021

PeneloPET, a Monte Carlo PET simulation tool based on PENELOPE: features and validation

S España[1], J L Herraiz[1], E Vicente[1,2], J J Vaquero[3], M Desco[3] and J M Udias[1]

[1] Grupo de Física Nuclear, Departmento de Física Atómica, Molecular y Nuclear, Universidad Complutense de Madrid, Madrid, Spain
[2] Instituto de Estructura de la Materia, Consejo Superior de Investigaciones Científicas (CSIC), Madrid, Spain
[3] Unidad de Medicina y Cirugía Experimental, Hospital General Universitario Gregorio Marañón, Madrid, Spain

E-mail: jose@nuc2.fis.ucm.es

Received 28 October 2008, in final form 31 January 2009
Published 25 February 2009
Online at stacks.iop.org/PMB/54/1723

Abstract

Monte Carlo simulations play an important role in positron emission tomography (PET) imaging, as an essential tool for the research and development of new scanners and for advanced image reconstruction. PeneloPET, a PET-dedicated Monte Carlo tool, is presented and validated in this work. PeneloPET is based on PENELOPE, a Monte Carlo code for the simulation of the transport in matter of electrons, positrons and photons, with energies from a few hundred eV to 1 GeV. PENELOPE is robust, fast and very accurate, but it may be unfriendly to people not acquainted with the FORTRAN programming language. PeneloPET is an easy-to-use application which allows comprehensive simulations of PET systems within PENELOPE. Complex and realistic simulations can be set by modifying a few simple input text files. Different levels of output data are available for analysis, from sinogram and lines-of-response (LORs) histogramming to fully detailed list mode. These data can be further exploited with the preferred programming language, including ROOT. PeneloPET simulates PET systems based on crystal array blocks coupled to photodetectors and allows the user to define radioactive sources, detectors, shielding and other parts of the scanner. The acquisition chain is simulated in high level detail; for instance, the electronic processing can include pile-up rejection mechanisms and time stamping of events, if desired. This paper describes PeneloPET and shows the results of extensive validations and comparisons of simulations against real measurements from commercial acquisition systems. PeneloPET is being extensively employed to improve the image quality of commercial PET systems and for the development of new ones.

1. Introduction

Monte Carlo simulations play an important role in positron emission tomography (PET) imaging, as an essential tool for the research and development of new scanners and for advanced image reconstruction. The availability of powerful computers has encouraged the use of PET-dedicated simulation codes in the last few years. Examples of areas that benefit from extensive simulations are the design of new PET scanners (Braem *et al* 2004, Heinrichs *et al* 2003), the development and assessment of image reconstruction algorithms (Herraiz *et al* 2006) and of correction techniques (Levin *et al* 1995), among other applications (Zaidi 2000, Ay and Zaidi 2006, Ortuño *et al* 2003, 2006, Torres-Espallardo *et al* 2008). Simulations make it possible not only to refine the design parameters of PET scanners, but they also help to identify bottlenecks regarding count rate, resolution, sensitivity, etc.

There are several Monte Carlo codes (for a short and recent review see Buvat and Lazaro (2006)) that simulate the transport of radiation through matter, e.g. GEANT4 (Agostinelli 2003), MCNP (Briesmeister 1993), EGS4 (Kawrakow and Bielajew 1998) and PENELOPE (Baró *et al* 1995, Salvat *et al* 2003). Either based upon these codes or in tables of photon cross-sections, a number of tools for PET simulation have been developed, such as SIMSET (Harrison *et al* 2003), PETSIM (Thomson *et al* 1992) or Eidolon (Zaidi *et al* 1998), based on MCNP, and GATE, based on GEANT4 (Jan *et al* 2004). Probably (Buvat and Lazaro 2006), one of the most widely known is GATE which, being based in GEANT4, can include a large variety of photon detectors and targets the large community of high energy and nuclear physics users that have acquaintance with GEANT4. GEANT4 is powerful and flexible enough to simulate PET scanners; however, its learning curve is both steep and long. A superficial knowledge of C++ is insufficient to optimally use GEANT4, and the installation process requires more than basic computer skills. This is why GATE was developed. GATE consists of hundreds of classes that provide useful functionalities for PET simulations. No C++ programming is involved and thus it is easier to learn and use, unless there is a need to create new classes to address specific problems.

We have chosen PENELOPE as the core of our PET simulation tool. PENELOPE is a Monte Carlo code for the simulation of the transport in matter of electrons, positrons and photons with energies from a few hundred eV to 1 GeV. It is then less generally aimed as GEANT4, but it suits well PET needs, it is fast and robust, and it is extensively used for other medical physics applications, particularly for dosimetry and radiotherapy (Sempau and Andreo 2006, Panettieri *et al* 2007). PENELOPE is written in the FORTRAN programming language.

1.1. Why another PET simulator?

The main purpose of our PET simulator is the optimization of the design of small animal PET scanners. Most often these scanners are made of multiple scintillator arrays read by Anger-like logic, arranged in complex geometries with millions of lines of response (LORs). In order to optimize the scanner design, many high-statistics simulations have to be made and studied, each of them with different scanner settings, such as for instance geometry (scanner diameter, crystal size), materials (scintillator, shielding and other scatter elements), electronics (integration time, dead time, coincidence window, pile-up rejection), etc. Thus, it is desirable to have the fastest possible simulation tool, capable of running in parallel in clusters of computers, and able to provide an easy way of executing many simulation instances with small changes of the scanner definition. The ample variety of detector configurations

allowed by the combination GEANT/GATE is appealing, but it comes at the cost of increased need for computing resources (Buvat and Lazaro 2006).

The FORTRAN language is highly standardized and it is available for many computer architectures aimed to scientific computing, to which FORTRAN compilers have been adapted and optimized for speed and accuracy. Written in FORTRAN, PENELOPE is bound to be both fast and portable. On the other hand, while still widely used by physicists and mathematicians, FORTRAN is not the most popular programming language among young researchers and lacks the object-oriented structure that is appealing when writing modular codes. On these grounds, we have developed PeneloPET, a FORTRAN package that allows us to easily define complete simulations of PET systems within PENELOPE. PeneloPET is capable of preparing sophisticated simulations just by editing a few simple input text files, without requiring knowledge of FORTRAN or any other programming language. Simulations prepared with PeneloPET are straightforward to run in parallel using clusters of computers.

1.2. Introduction to PeneloPET

The basic components of a PeneloPET simulation are detector geometry and material definition (including non-detecting materials, like shielding), source definitions, non-active materials in the field of view (FOV) of the scanner and electronic chain of detection. All these components are defined with parameters in the input files. Different levels of output data are available for analysis, from sinogram and LORs histogramming to fully detailed list mode. These data can be further exploited with the preferred programming language, including ROOT. The detailed list mode generates a file with all the hits, single or coincidence events and the corresponding information about interaction coordinates, deposited energy in the detectors, and time and type of coincidence: random, scatter, true, with pile-up, etc.

In this work we have performed several comparisons with another PET-dedicated code (GATE) and with studies obtained from four commercial PET scanners. The agreement between PeneloPET simulations and the results obtained in real scanners confirms PeneloPET as a powerful tool for PET research and development as well as for quality assessment of PET images. PeneloPET is freely available and can be obtained by request from the authors. The reader interested can visit http://nuclear.fis.ucm.es/penelopet for details.

2. PeneloPET features

2.1. Source code

Our goal with PeneloPET has been to develop an easy-to-use program that includes all the physical and electronic processes involved in PET. PeneloPET requires a moderate time investment for the preparation of the simulation setup and it runs very efficiently, with modest computational burden compared to other PET simulation tools. It can be ported to any platform and operating system capable of compiling FORTRAN programs. We have tried PeneloPET under Windows, Linux/Unix and Mac OS X platforms and with different FORTRAN compilers (gnu-g77[4], Absoft[5], Intel[6]) without porting problems.

The source code consists of two main modules. The first one deals with the PENELOPE simulations and the level of detail chosen for these, and takes care of the information about scanner detectors and materials, source and decay. This module includes the routines involved

[4] http://www.gnu.org/software/fortran/fortran.html.
[5] http://www.absoft.com/Absoft%20Compilers.htm.
[6] http://www.intel.com/cd/software/products/asmo-na/eng/compilers.

in the distribution of isotopes and emission of particles generated in the decay processes as well as their interactions.

The second module post-processes the decay and interaction data generated by the first module. It takes into account, for instance, Anger logic for positioning the interaction inside the crystal array, detector pile-up, energy resolution in the scintillator and aspects of the electronics, such as coincidence time window, dead time, time resolution and integration time. No PENELOPE routines are generally involved in this second module. Energy windows can be applied in this second module. Continuous or pixelated detectors can be managed by this second stage of the simulation package.

In order to run the simulations on clusters of computers, a simple and portable Python[7] script is provided with the code. The use of Python enables one to run the script under Windows, Linux/Unix and Mac OS X. After configuring PeneloPET for the execution of the desired setup in a single CPU, the Python script launches the simulation on the number of CPUs desired, with different random seeds, and takes care of the initial activity and the acquisition time for each sub-process, in order to simulate the same number of decay events as the equivalent single-CPU run. In this way, the simulation time is reduced proportionally to the number of CPUs employed.

2.2. Input files

Four input files have to be prepared by the user in order to set up a simulation. The first input file (main.inp) contains the general parameters of the simulation, such as the acquisition protocol and acquisition time. It also selects the simulation of secondary particles, if desired, and controls whether the positron range and non-collinearity are taken into account. This file also contains options for scanner rotation, energy and coincidence windows, contributions to dead time, output format and type of study.

In the second file (scanner.inp), which contains the scanner definition, multiple rings and layers of crystals can be specified. Although our main goal was to simulate pixelated detectors for high-resolution small animal PET imaging, PeneloPET is also suitable for continuous scintillator blocks or even detectors not based on scintillators (such as CZT or silicon strips) with small or no changes.

Non-radioactive materials other than the scintillator (already defined in the file scanner.inp), such as the surrounding materials and shielding, are defined in a third file (object.inp). The radioactive source is defined separately in a fourth input file (source.inp), which contains source geometry and information about activity and isotope. Keeping separated definitions for sources and materials simplifies the comparison of simulations of ideal sources, without scatter or attenuation, and more realistic sources. All the details about PeneloPET input files and options can be found in the PeneloPET manual.[8]

Typical materials for crystals, shielding and phantoms are predefined in PeneloPET and, if necessary, new materials can be created in a straightforward way. The visualization tools built in PENELOPE (gview2d, gview3d (Salvat *et al* 2003)) are also available in PeneloPET to display and test geometries. This is especially useful during scanner design stages (see figure 1).

Although the examples presented in this work deal with pre-clinical scanners, PeneloPET is also capable of simulating clinical PET scanners.

[7] http://www.python.org/.
[8] http://nuclear.fis.ucm.es/penelopet/.

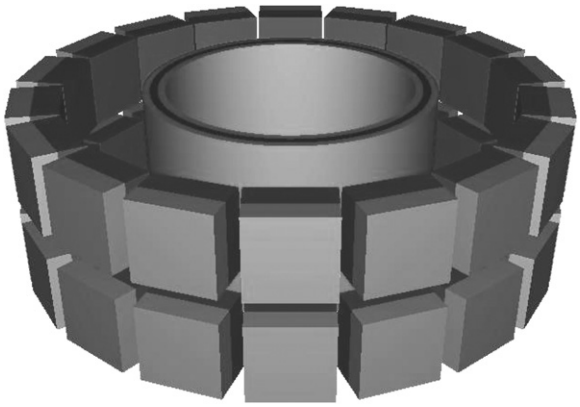

Figure 1. View of the SUINSA ARGUS (Wang *et al* 2006) scanner obtained with the gview3d application distributed with PENELOPE. An annulus phantom can also be observed, centered in the FOV.

2.3. Output

Output files generated by PeneloPET can offer three different levels of detail. At the highest level, all the information about each interaction is recorded for further analysis. At the intermediate level, just the single events and the information needed for their analysis is recorded. The possibility of pile-up and cross-talk is taken here into account. At the third, and lowest, level of detail, only coincidence events are recorded in a compact LIST mode. Information about pile-up, scatter, random and self-coincidence events obtained from the simulation is also summarily available.

A coincidence event is labeled as pile-up when at least one of the single events has suffered pulse pile-up. A coincidence is considered to be a scatter coincidence when at least one of the photons that trigger the detectors has interacted before reaching the scintillator. A coincidence is considered as a random one when the two photons in the coincidence pair come from two different, uncorrelated, annihilation process. A self-coincidence event may arise when the same photon, after scattering in a first detector, reaches a second detector. If the energy deposited in each detector is above the detection threshold, it may trigger two single events and yield a self-coincidence. The remaining coincidences are considered as true events.

PeneloPET generates several output histograms that help to understand the results of the simulations, such as for instance sinogram projections, LOR histogram, single and coincidence maps and energy spectrum. In order to simplify the reconstruction of simulated data, the format of the sinograms conforms to that expected by the STIR library.[9]

ROOT (Brun and Rademakers 1997) is an object-oriented data analysis framework that provides tools for the analysis of experimental data. PeneloPET LIST files can be converted into ROOT format. As an example, figure 2 shows a two-dimensional energy histogram of the single events that yield the coincidence events, which has been plotted with ROOT.

2.4. Geometry

The geometry of detectors and other materials of the scanner can be defined in the input files by means of a few text lines. The scanner definition file (scanner.inp) contains the description

[9] http://stir.sourceforge.net.

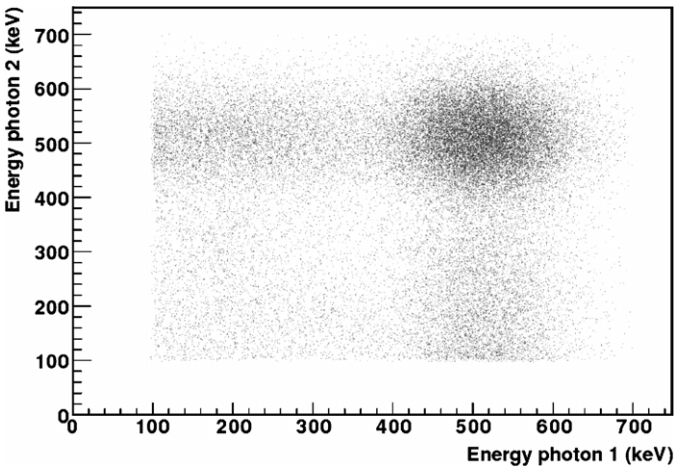

Figure 2. A two-dimensional energy histogram of single events belonging to the same coincidence, histogrammed with ROOT from the file generated with the ROOT-output option of PeneloPET.

of a multi-ring arrangement of rectangular prism-shaped detectors, often segmented into pixel crystals and with one or more layers of scintillator in each detector. Several predefined materials can be used in the detectors, and more materials can be defined by indicating their energy and time resolution and light pulse rise and fall time. Thus, the scanner definition includes the number of detectors per ring, number of rings, gap between adjacent rings, number of pixel crystals per detector, detector material, number of scintillation layers and material for each, pitch size and ring size. Other structures can be defined (object.inp) to complete the geometry with shielding and other non-detecting materials.

If the user needs to simulate more complex geometries, the geometry file can be directly created employing PENELOPE geometry syntax. Detector blocks can be displaced from their regular positions in order to build non-regular complex geometries or to introduce misalignments of detectors.

The distribution of radioactive sources used in the simulation is described in a third file (source.inp). It contains the shape, location, activity, radioactive isotope and restrictions in emission directions, if any.

2.5. Emission of annihilation photons

When annihilation photons are emitted, the direction of emission is randomly and isotropically generated. For some simulations it may be useful to restrict the allowed solid angle for the emission of photons, thus increasing the time efficiency of the simulation. Limits and/or privileged directions can be selected in the input files. PeneloPET automatically adjusts the simulation results according to the solid angle restrictions incorporated.

2.6. Isotope and source selection

Another input file (isotope.inp) contains the definition of one or several isotopes, stating the half-life and a list of all emitted particles as the nuclide decays. For each particle in the list, its type (electron, positron or photon), energy (Q_β, E_υ) and branching ratio are defined. Any mixture of sources with different isotopes and activities can be used as radioactive

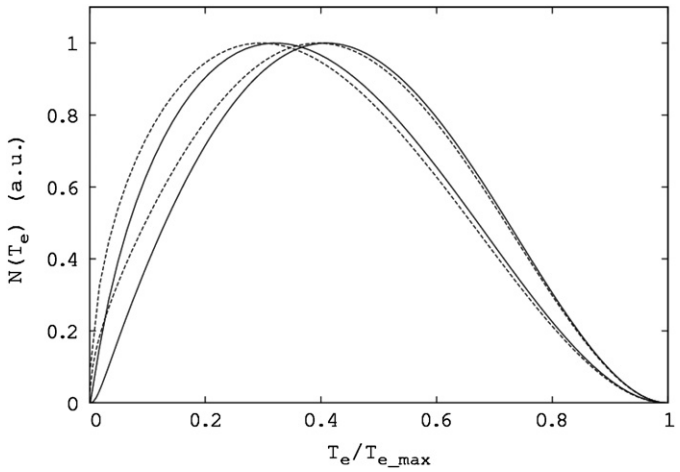

Figure 3. Simulated positron spectra obtained with PeneloPET and employed in positron range calculations. From left to right, ^{18}F, ^{68}Ge/^{68}Ga, dashed lines without Coulomb correction, solid lines with Coulomb correction. The horizontal axis represents the kinetic energy normalized to the maximum value of each spectrum.

distribution. The isotopes most commonly used in PET are already defined and it is easy for the user to define new ones if required. Time intervals between consecutive decays are randomly generated following statistical distributions appropriate to initial activity and decay time. Intrinsic activity of detectors can be included in the simulation by simply defining a source with the geometry and activity of the scintillator crystals.

2.7. Positron range

When a positron is generated in a decay process, it has a kinetic energy that depends on the energy shared with the neutrino created in the same process. This yields a continuum energy spectrum distribution which is easily computed from theoretical grounds, either for allowed or superallowed transitions, and including the Coulomb correction factor (see for instance equation (13) in Levin and Hoffman (1999)) after Richardson and Kurie (1936). In PET positron range simulations, this latter Coulomb correction factor is often either neglected or only treated with a non-relativistic approach. PeneloPET uses the exact expression for the Coulomb correction factor, which, albeit relatively close to one for light nuclei and positron emission, it may significantly distort the beta spectrum for medium to heavy nuclei, particularly in the case of electron emission. Figure 3 shows the normalized positron spectra corresponding to ^{18}F, and ^{68}Ge/^{68}Ga, with and without Coulomb correction.

PeneloPET offers two approaches for simulating the positron range. The first one tracks the path and energy spectrum for each positron coming from the decay process. This leads to accurate results, but at the expense of increased computation time. With the second approach, the profile of the positron range in water is generated from a detailed simulation (as described for the previous approach) only once, saving the resultant profile for later use in simulations in which the positron annihilation point will be randomly generated from these pre-computed profiles (Levin and Hoffman 1999, Harrison *et al* 1999). Positron range profiles for the β^+ isotopes most widely used in PET are included with PeneloPET. Profiles for other isotopes can be added using tools provided with PeneloPET.

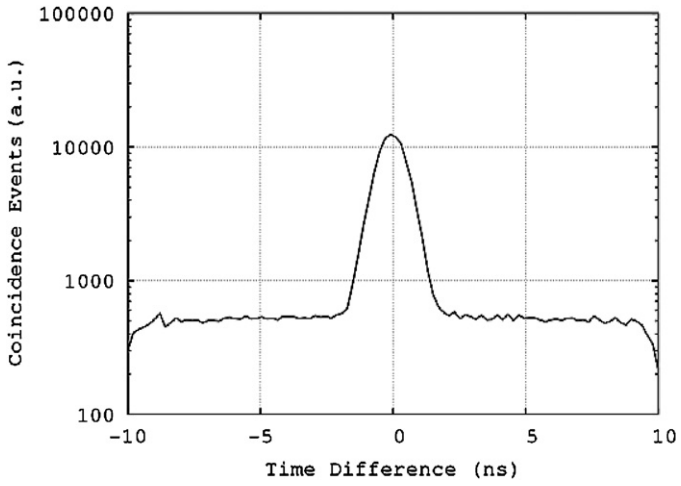

Figure 4. Histogram of time differences of the two single events in a coincidence pair. This simulation was performed using a rat-size phantom filled with 71 MBq of ^{18}F for the ARGUS scanner. The vertical axis is in logarithmic scale.

2.8. Non-collinearity

When an annihilation process takes place with both positron and electron at rest, two photons of about the same energy (511 keV) are produced. Because of energy and momentum conservation, both photons should be emitted along the same line but in opposite directions. However, annihilation usually takes places with thermal electrons which have a kinetic energy of a few eV, leading to a slight non-collinearity of the two emitted photons. This non-collinearity is modeled by a Gaussian distribution of 0.5 degrees FWHM (Harrison *et al* 1999).

2.9. Energy and time resolution, crystal assignment, coincidence window

Energy resolution of the detector at 511 keV is specified by the user in the scanner.inp input file and it is linearly extrapolated for other energies. Detector time resolution is estimated from time-blurring effects after a photon produces a trigger in a detector. Usual contributors to this time blurring are electronic jitter and rise time of the light emitted by the crystal detector. Furthermore, the simulations include the determination of the position of interaction by means of Anger-like center of gravity methods. To account for further blurring effects in the interacting pixel assignment, Gaussian blurring can be added to the final pixel assignment. Since all the events are time stamped, software cuts (time coincidence windows) can be applied to the listed events to select true coincidences. The list file generated by the simulation contains detailed time information for the events, so histograms of time differences between the two single events of a coincidence are easily created (see figure 4) and thus the efficiency of time coincidence cuts or even the probability that a coincidence count comes from a true or a random coincidence, given their time difference, can be readily estimated. The time information for the recorded counts can also include the time path of the photons from the decay point to the detectors, and thus time of flight (TOF) studies can be easily simulated. The user can arrange the simulated counts into TOF bins and use them in TOF reconstructions.

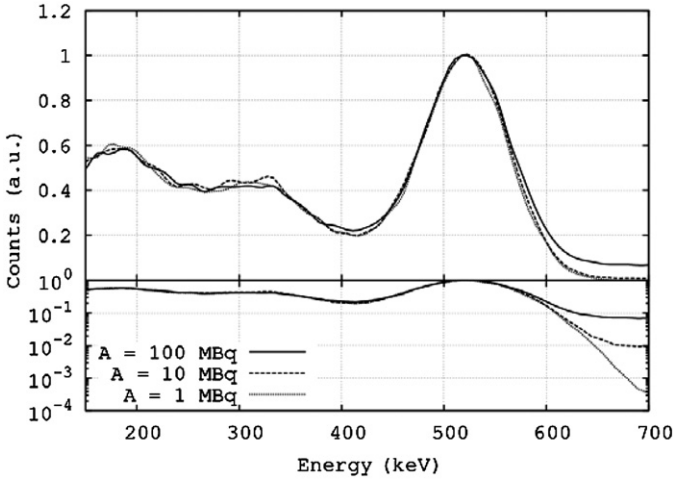

Figure 5. Energy spectrum for simulated acquisitions at different activity levels, with linear (top panel) and log (bottom panel) scales. This simulation was performed for a rat-size phantom filled with ^{18}F in the ARGUS scanner. Counts at the right of the photopeak are due to detector pile-up events, whose contribution is more conspicuous for larger activities. Pile-up events also fill in a bit the region around the Compton edge.

2.10. Pulse pile-up

A pulse is generated when a photon deposits energy in a detector above a given threshold. The shape and duration of this pulse are defined in the simulation. Due to the time response of the scintillator, an integration of the pulse during, typically, a hundred of nanoseconds is needed in order to measure the energy deposited by the photon and to localize the interaction. If any other photon interacts with the same detector within this integration time, an overlap of both pulses (detector pile-up) will result. Pile-up causes incorrect energy and crystal identification. The time response of the detectors and the acquisition electronics are taken into account in the simulations, and PeneloPET can also simulate mechanisms for pulse pile-up rejection. Figure 5 shows the distortion of the energy spectrum due to pulse pile-up obtained from PeneloPET simulations.

2.11. Dead time

Dead time occurs when new events take place while the acquisition chain is still busy analyzing previous events. In general, there are several sources of dead time in PET detectors. First of all, in the detection process, a trigger is activated when the energy deposited by a photon in the detector exceeds certain energy threshold. When this happens, new events may not be accepted during a certain amount of time. This constitutes the detector trigger (or single event) contribution to the total dead time of the scanner and it is usually small compared to other contributors to dead time. Some scanners (e.g. CLEARPET) work in single-mode acquisition, that is, every single event identified is converted while coincidence sorting is performed later. In this case, for every single event, additional dead time contributions should be considered. These include for instance integration time, explained in previous subsection, and also conversion time, that is, the time required to complete the analog to digital conversion (ADC) of the detector signals and the subsequent transmission and storage of this digital

information in a computer. In single-mode acquisition scanners, there may be no further contribution to dead time due to the subsequent processing and sorting of coincidences, as this can even be done off-line. On the opposite side, in many other scanners (e.g. VrPET or INVEON), the single events identified (i.e. free from detector trigger dead time) follow further processing (including ADC) only if they lie within a certain time coincidence window of another single event. This can be termed as coincidence-mode acquisition. In this case, the major contribution to total scanner dead time originates in the processing (most importantly ADC) and sorting of the events identified as members of a coincidence pair, and it is this 'coincidence dead time' the main contributor to the total dead time of the scanner. All these sources and types of dead time can be simulated in PeneloPET as it considers trigger and coincidences dead time, as well as integration time, separately in the main.inp file.

2.12. Constraints in energy and type of particle

PeneloPET offers all the possibilities of PENELOPE for introducing constraints in energy and kind of particle considered in the simulation (Baró *et al* 1995, Salvat *et al* 2003). Depending on the purpose of the simulation, the user may choose to track all the photons, electrons and positrons, including every secondary particle, or just some of them. It is also possible to track only the particles with energy above a certain threshold or to stop tracking a particle when its energy falls below a low energy threshold. Faster simulations can be performed by tracking only the annihilation photons. This may constitute a good approximation as far as the mean free path of secondary particles is short enough, as it is the case in medical imaging.

2.13. System response

Iterative reconstruction methods require knowledge of the system response matrix (SRM) (Herraiz *et al* 2006). The SRM is made up of elements representing the probability of detecting events coming from a given voxel in a given LOR. PeneloPET includes the possibility of building the SRM for specific LORs. For this purpose, a point source of the selected isotope is simulated in different locations along the channel of response (CHOR), defined as the region of the space associated with the LOR, in the sense that a source located anywhere inside the CHOR has a non-negligible probability of producing coincidence events in the detector defining the LOR (Herraiz *et al* 2006). Several parameters of the simulation can be tuned to establish a tradeoff between speed and accuracy. The SRM can also be obtained for rotating scanners, by calculating probabilities of detection for sinogram bins instead of LORs.

3. Validation of PeneloPET

This section presents and evaluates simulations generated by PeneloPET. First, a comparison between results obtained with PeneloPET and those provided by the GATE simulation toolkit is shown. An axial sensitivity profile for a simple configuration based on the rPET (Vaquero *et al* 2005) scanner was estimated from PeneloPET and GATE simulations. In the remainder of this section, we compare simulated measurements with real measurements for four commercial small-animal PET scanners: rPET (Vaquero *et al* 2005), ARGUS (Wang *et al* 2006), Raytest CLEARPET (Heinrichs *et al* 2003) and Siemens INVEON (McFarland *et al* 2007). The real measurements from ARGUS, CLEARPET and INVEON scanners were taken from Wang *et al* (2006), Sempere Roldan *et al* (2007) and Blake *et al* (2006), respectively. The simulations tried to reproduce as accurately as possible, with the information available to the authors, the geometry and materials mentioned in said references.

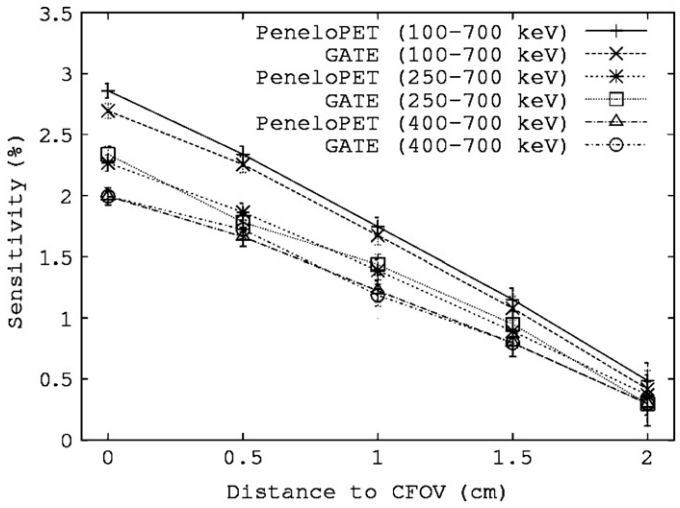

Figure 6. Axial sensitivity profile of the rPET scanner obtained from simulations of a low activity ^{18}F point source. PeneloPET results agree with those obtained with GATE within error bars except for the energy window with the lowest energy threshold, for which GATE sensitivities are larger than PeneloPET ones by about 5%. The error bars are taken as ± the standard error obtained from four runs of the simulations with different random seeds.

3.1. SUINSA rPET

rPET (SUINSA Medical Systems, Vaquero *et al* 2005) is a rotating scanner consisting of four PMT detector modules, each coupled to a single layer array of 30 × 30 MLS (Pepin *et al* 2001) crystals. Pitch size is 1.6 mm, individual crystal length is 12 mm and the ring diameter is 16 cm. A point source has been simulated at several axial positions along the axis of the FOV. Figure 6 shows the ratio of detected coincidences to annihilations at the source for three different energy windows. Source activity was kept low enough so that dead time, random and pile-up effects could be considered negligible. The simulation rates, measured as the number of positron (e^+) annihilations simulated per second using an Intel Xeon X5472 3.00 GHz quad-core processor, were 75 000 e^+ s^{-1} and 12 000 e^+ s^{-1}, for PeneloPET and GATE codes, respectively. In both cases, only annihilation photons of 511 keV were simulated, no angular restrictions were imposed and neither secondary particles nor x-rays were considered. The simulation rate depends strongly on the geometry of the scanner, shielding and surrounding materials included in the simulation. A similar simulation of the same source done for the other scanners studied in this work obtained 12 000 e^+ s^{-1} for ARGUS, 12 000 e^+ s^{-1} for CLEARPET and 17 000 e^+ s^{-1} for INVEON, a much lower simulation rate than the one obtained for rPET.

Regarding the accuracy of the results, there are small quantitative differences (about 5%) between the sensitivity predictions in the case of the 100–700 keV energy window. For the GATE simulations, the GEANT4 standard electromagnetic (EM) model was chosen. Three EM models are available in GEANT4, and thus also in GATE: the standard one, the low energy one and the same PENELOPE model that we employ in PeneloPET. It has been found in several works that these three models produce slightly different predictions (Poon and Verhaegen 2005). Some authors (Chen *et al* 2006) have suggested that the PENELOPE model may be more adequate for Compton interactions, the low-energy model for Rayleigh scattering

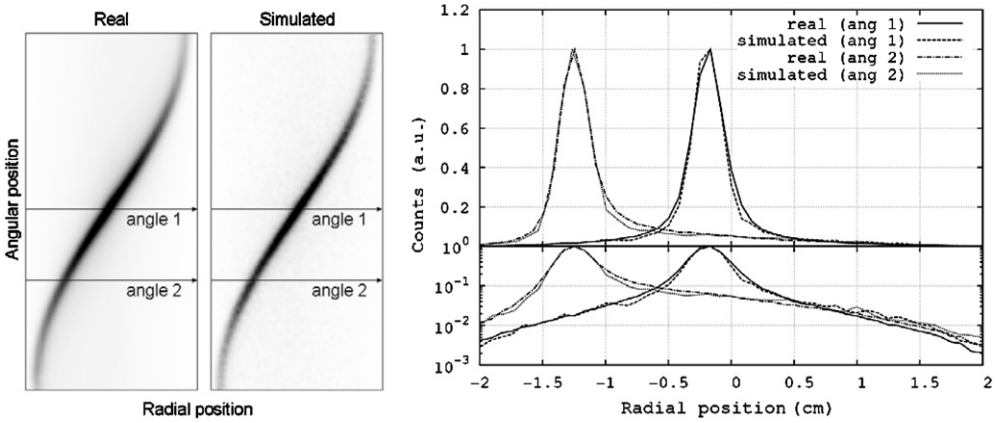

Figure 7. Comparison of real and simulated sinograms of a water-filled cylinder plus an off-centered rod with ^{18}F (250 μCi) for the rPET scanner. Radial profiles at two different angular positions are presented in the right panel with both log (bottom part of the figure) and linear vertical scales. The two arrows in the sinogram of the left panel indicate where the radial profiles shown in the right panel were taken. Simulated and real line profiles are scaled to coincide at their maximum values.

and the standard EM model of GEANT4 for photoelectric absorption of photons. One must be aware that we simulate the interaction of annihilation photons not only with biological tissue, but also with detector materials, such as scintillator and shielding. Thus, Compton and photoelectric absorption of photons are equally relevant for our simulations. In any case, the differences between these three models are not large, except for the lowest energy photons, which are of little relevance for the results of PET simulations.

Additionally, real and simulated sinograms from a mouse phantom acquisition were compared. The real acquisition was performed at Hospital General Universitario Gregorio Marañón, in Madrid. The mouse phantom was made of a rod filled with ^{18}F, 1 cm off-centered in a water cylinder of 2.5 cm of diameter and 6 cm in length. For this comparison we show the radial profiles of coincidences for two different angles. The initial activity was 250 μCi and no energy window was applied. Figure 7 shows that there is good agreement between real and simulated data in both peak and background areas.

3.2. SUINSA ARGUS

The ARGUS small-animal PET scanner (Wang *et al* 2006) consists of 36 PMT detector modules, each coupled to a dual layer array of 13 × 13 LYSO + GSO scintillation crystals. Each pixel crystal has a cross-section of 1.45 × 1.45 mm^2 separated by a white reflector 0.1 mm thick. The resulting pitch size is 1.55 mm and the length of the LYSO and GSO layers is 7 mm and 8 mm, respectively. The 36 modules are arranged in two rings of 18 modules each, with a diameter of 11.8 cm. All the measurements described in this section are taken from Wang *et al* (2006) except the one regarding the annulus phantom, which was obtained at Hospital General Universitario Gregorio Marañón, in Madrid.[10]

[10] The Argus scanner is described in Vaquero *et al* (2004). eXplore VISTA is the commercial name given by GEHC to the original SUINSA product, the ARGUS PET. These two systems are identical except for the identification logos on the system cover. The measurement mentioned here has been done using an ARGUS SUINSA system.

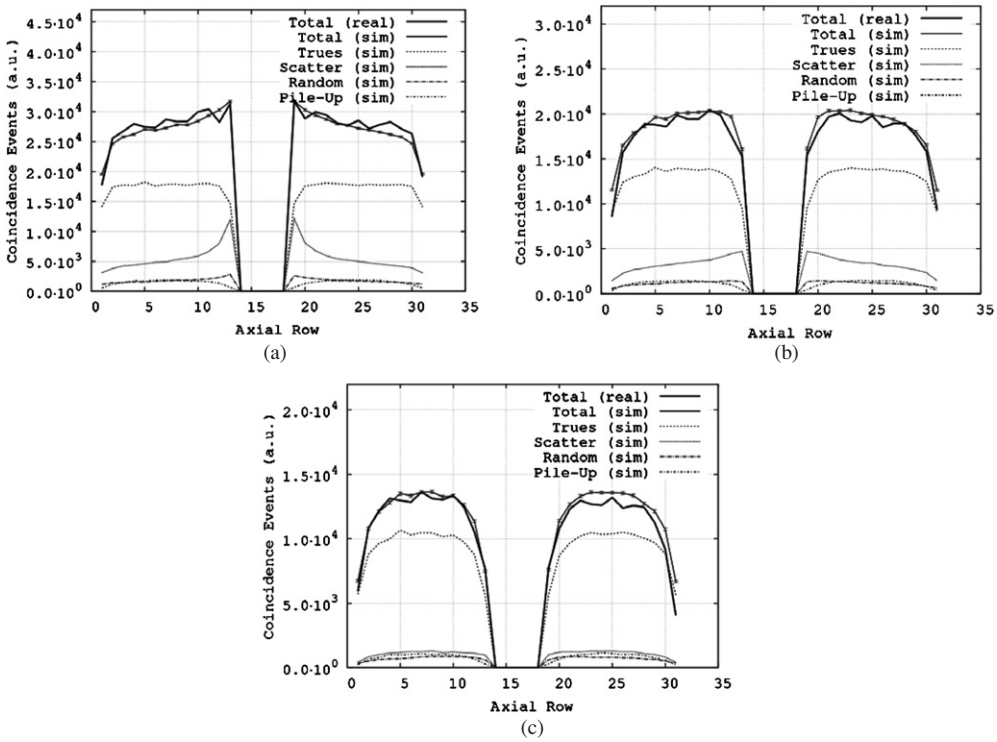

Figure 8. Comparison of the profiles of coincidence counts for crystals in the same axial row from a 500 μCi ^{68}Ge annulus. Different energy windows are shown: (a) 100–700 keV, (b) 250–700 keV and (c) 400–700 keV. Real (thick solid lines) and simulated (thin solid line) results from PeneloPET are presented. Also, for the simulations, contribution of true, random and scatter counts, as well as counts that are affected by detector pile-up are displayed separately. The small error bars (visible only in the simulated profiles) indicate the expected statistical error. Real and simulated line profiles are scaled to coincide at their maximum values.

For the first measurement, an annulus phantom made of epoxy containing ^{68}Ge was acquired. This annulus is normally employed to perform normalizations and calibrations of the scanner. It has an inner diameter of 6.92 cm, its walls are 2 mm thick and its total activity is about 500 μCi. Acquisitions were obtained with three energy windows (100–700 keV, 250–700 keV and 400–700 keV). Figure 8[11] shows a comparison of count profiles resulting from all coincidence events coming from crystals in the same axial row, with the ones from the simulation. The overall shape of these profiles is well reproduced by the simulations. The discontinuity at the center of the profile is due to the gap between the two detector rings. Both real acquisition and simulations have a very large number of events, so that the statistical error is negligible. The ripple observed in the real profiles may be due to a non-uniform axial distribution of shielding and other scanner materials, combined with edge effects of the PMTs, and with the unavoidable (although small) differences in the positions of the real crystals with respect to their *ideal* locations. In the simulation, ideal geometries for the crystal arrays, PMTs and photocathodes, as well as shielding, have been employed. It is thus reasonable to expect a more uniform axial structure for the profile of simulated counts than that exhibited by an

[11] In this work the term 'statistical error' denotes the variation in the measured magnitude induced by statistical fluctuations, that is, a variation of $\pm\sqrt{N}$, with N being the number of counts accumulated for said measurement.

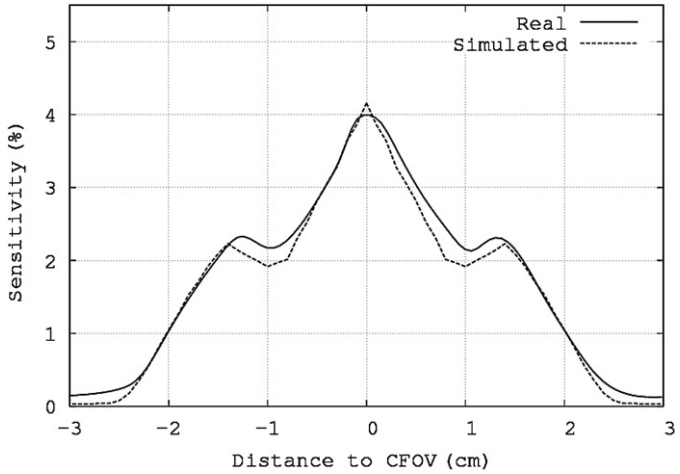

Figure 9. Axial sensitivity profile of the ARGUS scanner measured with a ^{18}F point source shifted in small steps along the central axis of the FOV, compared to PeneloPET simulations. Data are from Wang *et al* (2006). The simulations include inert material and shielding.

Table 1. Scatter fraction for the ARGUS scanner.

Energy window	Mouse phantom		Rat phantom	
(keV)	Real	Simulated	Real	Simulated
100–700	33%	29%	48%	42%
250–700	27%	27%	37%	38%
400–700	19%	20%	29%	29%

actual machine. In any case, this ripple observed in the real acquisitions is about 5% and the difference observed with the simulated results is of the same order.

We can notice a change in shape of the axial profiles according to the energy window selected. From the simulations we can obtain separated contributions to the axial count profiles from true, random and scatter counts, as well as from counts that are affected by pile-up. According to the simulations, we can attribute the largest contribution to this change in shape of the profiles to scatter counts. Further, there is a noticeable difference in the fraction of scatter coincidences registered with the 100–700 keV energy window, as compared to the narrowest one (400–700 keV).

Table 1 presents the results for the scatter fraction, real and simulated with PeneloPET. Real values were taken from Wang *et al* (2006). Differences between real and simulated values are below 5% for both the 250–700 and 400–700 keV energy windows. For the 100–700 keV energy window, the simulated values are systematically lower (by about 10%) than the real ones, most likely due to the fact that the simulations did not include secondary particle emissions, such as x-rays, that can contribute at low energies. The expected relative statistical error obtained from the simulations is $\pm$5%.

Figure 9 shows the comparison of simulated axial sensitivity profiles against real data from the ARGUS scanner. The agreement of the simulations with the data is very good at the center of the scanner (they agree within 5%), while there are somewhat larger differences (about 10%) in the relative minima of the sensitivity profile corresponding to the centers of

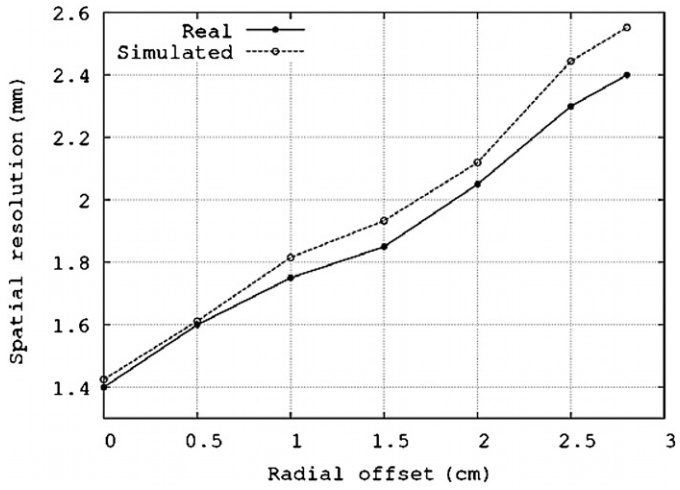

Figure 10. Radial resolution of the ARGUS scanner measured with a ^{22}Na point source placed at different radial positions in the central axial slice.

Table 2. Peaks of the NECR curve of a rat-size phantom for three energy windows, for the ARGUS scanner.

NECR (kcps) [activity (kBq/cc)]	100–700 keV	250–700 keV	400–700 keV
Real	120 [92]	140 [78]	145 [43]
Simulated	125 [86]	130 [74]	150 [40]

each ring. Outside these two minima, the differences between simulations and real data are below 5%. Overall, the agreement between simulation and data is good.

Figure 10 presents a comparison of the radial resolution measured for a ^{22}Na point source placed at different radial distances from the scanner axis, for real and simulated data. The resolution obtained from the simulation is in very good agreement with the experimental data at the center of the FOV (CFOV), while for larger offsets small deviations (of no more than 7%) can be observed.

Finally, simulations to obtain the noise equivalent count rate (NECR) for a rat-size phantom have been performed. NECR peak values obtained from real data were taken from Wang *et al* (2006). NECR data simulated from PeneloPET were analyzed to find the position of the NECR peak. Agreement of simulated and real NECR values simulated is good, as shown in table 2. Due to the fact that a finite number of steps are employed to find the maximum of the NECR curves, we estimate that these figures are affected by a relative error lower than 5% in both position and value of the peak.

3.3. Raytest CLEARPET

The CLEARPET (Heinrichs *et al* 2003) scanner consists of 80 PMT detector modules, each coupled to a dual layer array of 8 × 8 LYSO + LuYAP scintillation crystals. Each pixel crystal has a cross-section of 2 × 2 mm^2 and there is a 0.3 mm thick reflector between them. Pitch size is 2.3 mm and the length of both LYSO and LuYAP layers is 1 cm. The 80 modules are arranged in four rings of 20 modules with a diameter of 13.5 cm. Every four contiguous

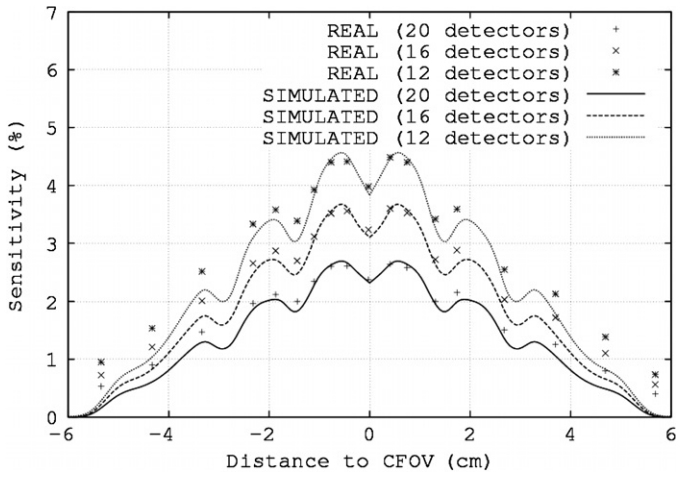

Figure 11. Axial sensitivity profile for the CLEARPET scanner. The figure shows measurements and results from simulations for three different scanner configurations (12, 16, and 20 detectors per ring) with a detector diameter of 13.5 cm. Real data are taken from Sempere Roldan *et al* (2007) and are represented with points.

modules in the axial direction form a *cassette*. Every second cassette is alternatively shifted by ±9.2 mm in the axial direction.

The axial sensitivity profile for the CLEARPET scanner was simulated for configurations with different number of detectors. Simulations of a ^{22}Na point source placed at many positions along the axial direction are compared to real data taken for 18 positions. The sensitivity was calculated as the ratio of the number of coincidence events measured inside the energy window of 250–750 keV and the total number of decays occurred during the acquisition time. Figure 11 shows the results of this comparison. There is good agreement in the central region of the axial profile, where simulation and data are within few percent of each other, and a worse agreement toward the edges of the axial FOV. This is most likely due to the fact that in this case the simulation did not include any shielding materials. The shielding materials can increase the number of events due to photons that first interact in the shielding and are then back scattered into a detector.

3.4. Siemens INVEON

The INVEON (McFarland *et al* 2007) consists of 64 PMT detector modules, each coupled to a single layer array of 20 × 20 LSO scintillation crystals. Each crystal has a section of 1.55 × 1.55 mm^2 and are separated with a 0.05 mm thick reflector. Pitch size is 1.6 mm and the length of LSO crystals is 1 cm. The 64 modules are arranged in four rings of 16 modules with a diameter of 16.1 cm.

An estimation of sensitivity of this scanner was made by means of a line source 14 cm long filled with 1.3 MBq of ^{18}F placed along the central axis of the scanner. The simulation included all the materials in the line source in order to take into account attenuation effects at the source. The sensitivity obtained for the line source activity was converted to equivalent sensitivity for a centered point source, as explained in Kemp *et al* (2006). The sensitivity estimated from real measurements by Kemp *et al* (2006) was 52.0 cps kBq^{-1}. The sensitivity estimated from the simulations was 52.7 cps kBq^{-1}, in good agreement with the real measurements.

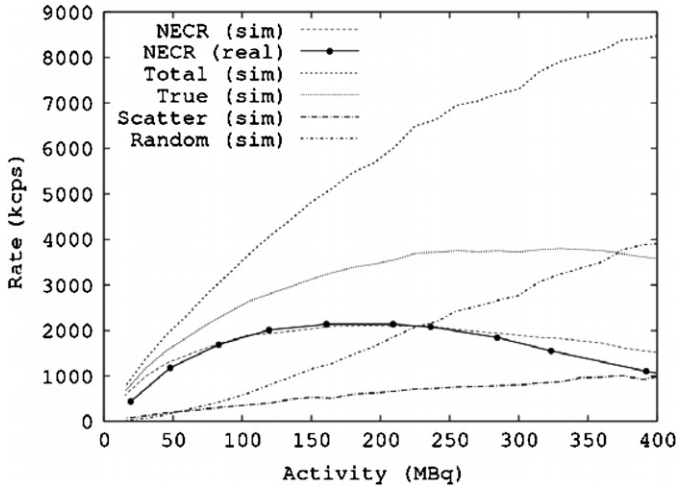

Figure 12. NECR curve for a mouse-size phantom acquired with the INVEON scanner. Simulated results are compared to the measurements of reference Kemp *et al* (2006). Total coincidence rates and true, scatter and random counts contribution are also shown for the simulation.

Figure 12 shows the NECR obtained from a simulation of a mouse size phantom of plastic material with a 3.6 mm hole, 1 cm off-centered. A line source filled with FDG is introduced in the hole and an acquisition with an energy window from 350 to 650 keV is performed. This simulation mimics the setup described by Kemp *et al* (2006) to measure the INVEON NECR curve. We have taken the acquisition performance parameters (time and energy coincidence window, etc) according to the values quoted by Kemp *et al* (2006). Figure 12 shows the components of NECR obtained from the simulation and the simulated NECR compared to the real measurements. Good agreement for the position of the NEC peak and the maximum NEC counts is found. Agreement is worse at higher rates, probably due to differences in dead time and pile-up rejection mechanisms of the real scanner and the ones included in the simulation.

4. Advanced use of simulations

Beyond the common uses of simulations for the determination of optimal scanner parameters and to obtain the system response, the availability of realistic and detailed simulations in reasonable computing time makes it possible to analyze the structure of the coincidence events registered by each scanner, estimating the reliability of each count, on an event by event basis. Indeed, with the help of detailed simulations, it is possible to establish a correlation between the parameters recorded by the scanner for each count, such as rate of coincidences and, if available, of singles too, XY-positioning of the interaction as provided by standard Anger algorithms, energy deposited in the detectors and the likelihood of the count acquired of being assigned to the correct crystal of first interaction. Details of this procedure have been given in España *et al* (2007b). Due to detector pile-up, coincidences acquired at high rates will suffer, more often than the ones at low rates, of wrong crystal positioning. Thus, the reliability of the crystal identification will not be the same for counts with low or high energy deposited in the detector. Similarly, counts with XY position information lying in the region between neighboring crystals will correspond more often to multicrystal events than counts with XY coordinates corresponding to the center of a crystal. A histogram of reliability (or percentage

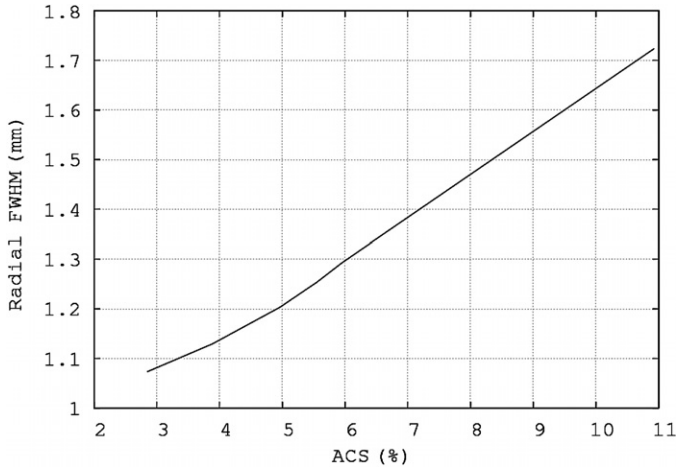

Figure 13. Radial resolution versus absolute sensitivity at the CFOV (ACS) obtained from a PeneloPET simulation of the INVEON scanner (see the text). The curve spans different reliability thresholds for the counts included in the reconstruction.

of counts assigned to the crystal of first interaction) as a function of XY-positioning information, time difference of the event pairs, singles and coincidence rates, energy deposited in each detector and other variables recorded by the scanner, can be built from simulations. Advanced acquisition and reconstruction systems could decide to process (or not) each count depending on the estimates of reliability. It could discard those counts whose reliability, for instance, falls below a certain threshold. This implies a loss of sensitivity, but it increases the ratio of counts correctly assigned to the crystal of first interaction, thus yielding better resolution. Simulations can be employed to produce diagrams of resolution versus sensitivity at the CFOV. Figure 13 shows a resolution versus sensitivity (the former estimated from FBP reconstructions of simulated acquisitions) curve for a point source in the center of the Inveon scanner. The curve is obtained changing the reliability threshold for the events accepted in the reconstruction. In one extreme, a very small threshold is employed so that essentially all events are accepted, in the high sensitivity (near 11%) end of the curve. In this case, simulations show that only 40% of the events are correctly assigned to the crystal of first interaction. In the other end of the curve, a very high reliability is required before accepting an event. This translates into more than 95% of accepted events being correctly assigned to the crystal of first interaction. In this case, the resolution is much better, but at the expense of using less than 30% of the counts. This causes the sensitivity to fall below 3%. The user could decide how to reconstruct a particular acquisition based on the resolution versus sensitivity trade-off of each scanner.

5. Conclusions

In this work, we present PeneloPET, an easy-to-use package for PET simulations. For its versatility, good simulation speed and easy-to-analyze outputs, PeneloPET is a useful tool for scanner design, system response calculations, development of corrections methods and other applications. We have also compared simulations of PeneloPET to real measurements from four different small-animal PET scanners. We have compared both integral or extensive properties of scanners, such as sensitivity, axial profile of counts, scatter fraction and NEC

rates, and intensive ones, namely sinogram profiles and spatial resolution, finding in general good agreement between simulated and real data. Simulations with PeneloPET differed from those of GATE by only a few percent and were considerably faster.

Acknowledgments

We acknowledge support from MEC (FPA2007-07393), CDTEAM (CENIT-Ingenio 2010) Ministerio de Industria, Spain, CPAN (Consolider-Ingenio 2010) CSPD-2007-00042 projects and the RECAVA-RETIC network. Part of the computations of this work were done at the 'High Capacity Cluster for Physical Techniques' of the Faculty for Physical Sciences of the UCM, funded in part by the UE under the FEDER program and in part by UCM. J L Herraiz and E Vicente acknowledge support from UCM-FPU and CSIC-JAE pre-doctoral fellowships, respectively.

References

Agostinelli S 2003 GEANT4—a simulation toolkit *Nucl. Instrum. Methods Phys. Res.* A **506** 250–303

Ay M R and Zaidi H 2006 Assessment of errors caused by X-ray scatter and use of contrast medium when using CT-based attenuation correction in PET *Eur. J. Nucl. Med. Mol. Imaging* **33** 1301–13

Baró J, Sempau J, Fernández-Varea J M and Salvat F 1995 PENELOPE: an algorithm for Monte Carlo simulation of the penetration and energy loss of electrons and positrons in matter *Nucl. Instrum. Methods Phys. Res.* B **100** 31–46

Blake E, Pressley D R, Lenox M, Swann B K, Newport D F and Siegel S 2006 A data acquisition, event processing and coincidence determination module for a distributed parallel processing architecture for PET and SPECT imaging *IEEE NSS MIC Conf. Rec.* pp 2439–42

Braem A *et al* 2004 Feasibility of a novel design of high resolution parallax-free Compton enhanced PET scanner dedicated to brain research *Phys. Med. Biol.* **49** 2547–62

Briesmeister J F 1993 MCNP 4. A Monte Carlo N-particle transport system *Report LA-12625* Los Alamos National Laboratory

Brun B and Rademakers F 1997 ROOT—an object oriented data analysis framework *Nucl. Instrum. Methods Phys. Res.* A **389** 81–6

Buvat I and Lazaro D 2006 Monte Carlo simulations in emission tomography and GATE: an overview *Nucl. Instrum. Methods Phys. Res.* A **569** 323–29

Chen Y, Liu B, O'connor M, Didier C S and Glick S J 2006 Comparison of scatter/primary measurements with GATE simulations for X-ray spectra in cone beam CT mammography *IEEE NSS MIC Conf. Rec.* pp 3909–14

España S, Herraiz J L, Vicente E, Desco M, Vaquero J J and Udias J M 2007a Validation of PeneloPET against two small animal PET scanners *IEEE NSS MIC Conf. Rec.* pp 3640–43

España S, Herraiz J L, Vicente E, Herranz E, Vaquero J J, Desco M and Udias J M 2007b Improved image reconstruction in small animal PET using a priori estimates of single-pixel events *IEEE NSS MIC Conf. Rec.* pp 3876–80

Harrison R L, Dhavala S, Kumar P N and Shao Y 2003 Acceleration of SimSET photon history generator module of a public domain simulation system for emission tomography *IEEE NSS MIC Conf. Rec.* pp 1835–8

Harrison R L, Kaplan M S, Vannoy S D and Lewellen T K 1999 Positron range and coincidence non-collinearity in SimSET *IEEE NSS MIC Conf. Rec.* pp 1265–8

Heinrichs U, Pietrzyk U and Ziemons K 2003 Design optimization of the PMT-ClearPET prototypes based on simulation studies with GEANT3 *IEEE Trans. Nucl. Sci.* **50** 1428–32

Herraiz J L, España S, Vaquero J J, Desco M and Udias J M 2006 FIRST: fast iterative reconstruction software for (PET) tomography *Phys. Med. Biol.* **51** 4547–65

Jan S, Santin G, Strul D, Staelens S, Assié K, Autret D and Avner S 2004 GATE: a simulation toolkit for PET and SPECT *Phys. Med. Biol.* **49** 4543–61

Kawrakow I and Bielajew A F 1998 On the condensed history technique for electron transport *Nucl. Instrum. Methods Phys. Res.* B **142** 253–80

Kemp B J, Lenox M, Newport D F, Siegel S and Nutt R 2006 Performance measurements of the Siemens Inveon small animal PET scanner *IEEE NSS MIC Conf.* poster presentation

Levin C S, Dahlbom M and Hoffman E J 1995 A Monte Carlo correction for the effect of Compton scattering in 3-D PET brain imaging *IEEE Trans. Nucl. Sci.* **42** 1181–5

Levin C S and Hoffman E J 1999 Calculation of positron range and its effect on the fundamental limit of positron emission tomography system spatial resolution *Phys. Med. Biol.* **44** 781–99

McFarland A R, Siegel S, Newport D F, Mintzer R, Atkins B and Lenox M 2007 Continuously sampled digital pulse processing for Inveon small animal PET scanner *IEEE NSS MIC Conf. Rec.* pp 4262–5

Ortuño J E, Guerra-Gutierrez P, Rubio J L, Kontaxakis G and Santos A 2006 3D-OSEM iterative image reconstruction for high-resolution PET using precalculated system matrix *Nucl. Instrum. Methods Phys. Res.* A **569** 440–4

Ortuño J E, Vaquero J J, Kontaxakis G, Desco M and Santos A 2003 Preliminary studies on the design and simulation of high resolution small animal PET scanners with octagonal geometry *IEEE NSS MIC Conf. Rec.* pp 2053–8

Panettieri V, Wennberg B, Gagliardi G, Duch M A, Ginjaume M and Lax I 2007 SBRT of lung tumours: Monte Carlo simulation with PENELOPE of dose distributions including respiratory motion and comparison with different treatment planning systems *Phys. Med. Biol.* **52** 4265–81

Pepin C M, Berard P and Lecomte R 2001 Comparison of LSO, LGSO and MLS scintillators *IEEE NSS MIC Conf. Rec.* pp 124–8

Poon E and Verhaegen F 2005 Accuracy of the photon and electron physics in GEANT4 for radiotherapy applications *Med. Phys.* **32** 1696–711

Richardson J R and Kurie F N D 1936 The rediations emitted from artificially produced radioactive substances. II. The gamma-rays from several elements *Phys. Rev.* **50** 999–1006

Salvat F, Fernández-Varea J M and Sempau J 2003 PENELOPE—a code system for Monte Carlo simulation of electron and photon transport NEA-OCDE

Sempau J and Andreo P 2006 Configuration of the electron transport algorithm of PENELOPE to simulate ion chambers *Phys. Med. Biol.* **51** 3533–48

Sempere Roldan P, Cañadas M, Dietzel O, Pautrot C, Sarasola I and Wagner A 2007 Performance evaluation of raytest ClearPET, a PET scanner for small and medium size animals *IEEE NSS MIC Conf. Rec.* pp 2859–64

Thomson C J, Moreno-Cantu J and Picard Y 1992 PETSIM: Monte Carlo simulation of all sensitivity and resolution parameters of cylindrical positron imaging systems *Phys. Med. Biol.* **37** 731–49

Torres-Espallardo I, Rafecas M, Spanoudaki V, Mcelroy D E and Ziegler S I 2008 Effect of inter-crystal scatter on estimation methods for random coincidences and subsequent correction *Phys. Med. Biol.* **53** 2391–411

Vaquero J J, Lage E, Ricón L, Abella M, Vicente E and Desco M 2005 rPET detectors design and data processing *IEEE NSS MIC Conf. Rec.* pp 2885–9

Vaquero J J, Pascau J, Molins A, Arco J M and Desco M 2004 Performance characteristics of the ARGUS-drT small animal PET scanner: preliminary results *IEEE NSS MIC Conf. (Rome, Italy, 2004) (Book of Abstracts)* p 148

Vilches M, García-Pareja S, Guerrero R, Anguiano M and Lallena A M 2007 Monte Carlo simulation of the electron transport through thin slabs: a comparative study of PENELOPE, GEANT3, GEANT4, EGSnrc and MCNPX *Nucl. Instrum. Methods Phys. Res.* B **254** 219–30

Wang Y, Seidel J, Tsui B M W, Vaquero J J and Pomper M G 2006 Performance evaluation of the GE healthcare eXplore VISTA dual-ring small-animal PET scanner *J. Nucl. Med.* **47** 1891–900

Zaidi H 2000 Comparative evaluation of scatter correction techniques in 3D positron emission tomography *Eur. J. Nucl. Med. Mol. Imaging* **27** 1813–26

Zaidi H, Labbé C and Morel C 1998 Implementation of an environment for Monte Carlo simulation of fully 3-D positron tomography on a high-performance parallel platform *Parallel Comput.* **24** 1523–6